

Reusable Energy-Absorbing Architected Materials Harnessing Snapping-Back Buckling of Wide Hyperelastic Columns

Yuzhen Chen and Lihua Jin*

A new class of reusable energy-absorbing architected material is developed by harnessing the snapping-back buckling of wide hyperelastic columns. Subjected to an axial compression, a wide hyperelastic column can discontinuously buckle, snapping from one stable equilibrium state to another, leading to energy dissipation, while upon unloading, it can completely recover its undeformed state. Making use of this property, an energy-absorbing architected material is designed by stacking layers of wide hyperelastic columns, and it is fabricated by multi-material 3D printing and sacrificial molding. Characterized by quasi-static and drop tests, the material shows the capability of energy dissipation and impact force mitigation in a reusable, self-recoverable, and rate-independent manner. A theory is established to predict the energy-absorbing performance of the material and the influence of the column geometry and layer number. Wide tunability of the peak force, energy dissipation, and stability of the material is further demonstrated. This work provides new design strategies for developing reusable energy-absorbing materials and opens new opportunities for improving their energy dissipation capacities.

of viscous flow^[4] and viscoelasticity^[5–7] can be used repeatedly, but they are highly rate-dependent with slow recovery to the undeformed states upon unloading. Friction^[8–10] between particles in granular materials also permits reusability, but the collapsed materials are usually not self-recoverable, i.e., they do not recover their undeformed states.

To achieve a reusable, rate-independent, and self-recoverable energy-absorbing material, a novel design strategy of harnessing the snapping-through instability of tilted or curved beams in architected materials has been proposed.^[11–28] These beams are stacked into a multi-layered structure, and buckle sequentially one layer after another under compression, resulting in a nearly constant force as the displacement proceeds. The impact energy can be either trapped in the material due to bistability, or damped into heat due to snapping motions. Since the material only

1. Introduction

Energy-absorbing materials are ubiquitously used to protect humans and objects from impacts or collisions, examples including football helmets, car bumpers, and packaging of delicate goods. The essence of an energy-absorbing material is the capability of absorbing mechanical shock energy while keeping the peak force below the safety threshold. Besides, energy dissipation is required to mitigate rebounds.^[1] Among various energy dissipation mechanisms, plastic deformation or fracture of metals, ceramics, and composites^[2,3] is often utilized to dissipate a large amount of energy by means of dislocation motion or bond breakage. However, these energy-absorbing materials are typically only good for one-time usage, since they undergo irreversible deformation or are permanently damaged during an impact. Materials with the energy dissipation mechanisms

deforms elastically, it is reusable and rate-independent. However, when the constituent beams are bistable,^[11–13,15,16,18,21,23,24] the architected material stays in the deformed configuration after compression, without self-recovering its undeformed state. On the other hand, when the constituent beams are monostable, although the formed energy-absorbing architected material is self-recoverable upon unloading, a large number of layers connecting in series are required to achieve energy dissipation,^[17,19,29] making the structure thick and heavy. Connecting a single curved beam with a tailored elastic element allows energy dissipation without building a multi-layered structure,^[30] but the complex design and the large volume of the elastic element make it unsuitable for practical applications.

In this paper, we report a new class of reusable, rate-independent, and self-recoverable energy-absorbing architected material harnessing the snapping-back buckling of wide hyperelastic columns. Our recent study^[31,32] shows that an axially-loaded column (**Figure 1A**) can exhibit continuous, snapping-through and snapping-back buckling modes as the width-to-length ratio of the column increases (**Figure 1B**). In particular, the snapping-back buckling is a new mode of column buckling, where the force–displacement relation is discontinuous under not only force-controlled, but also displacement-controlled loading. When axially compressed, the column can snap between different stable equilibrium states, leading to

Y. Chen, Prof. L. Jin
Department of Mechanical and Aerospace Engineering
University of California, Los Angeles
Los Angeles, CA 90095, USA
E-mail: lihua.jin@seas.ucla.edu

 The ORCID identification number(s) for the author(s) of this article can be found under <https://doi.org/10.1002/adfm.202102113>.

DOI: 10.1002/adfm.202102113

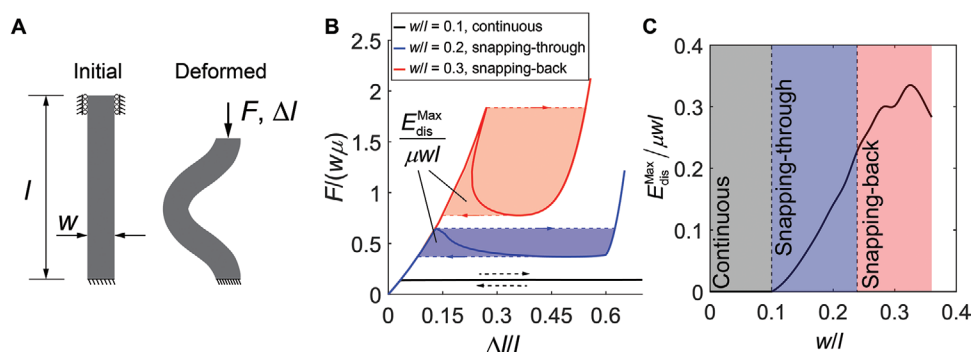


Figure 1. Energy dissipation mechanism of wide hyperelastic columns. A) Schematic drawing of a straight hyperelastic column with a width-to-length ratio w/l subjected to axial compression and the clamped–clamped boundary condition. The column buckles under a critical load or displacement. B) Normalized compressive force–displacement curves for three different values of w/l . The shaded areas indicate the normalized energy dissipation in one force-controlled loading and unloading cycle, which is also the maximum dissipated energy for the columns under displacement-controlled loading, $E_{\text{dis}}^{\text{max}}/\mu wl$. C) $E_{\text{dis}}^{\text{max}}/\mu wl$ as a function of w/l . The regions of different colors indicate the different buckling modes of the column.

energy dissipation. Upon unloading, the column instantaneously and completely recovers its undeformed state. Similar to tilted or curved beams that exhibit the snapping-through buckling, the wide hyperelastic column is reusable and rate-independent. However, compared to a tilted or curved beam, the wide column of the same geometry has a higher critical strain for buckling, and thus has a higher energy-absorption capacity. Moreover, due to the nature of the snapping-back buckling mode, the dissipated energy for the wide column stacked in series increases faster with the layer number than that for the tilted or curved beam. The strategy of harnessing the snapping-back buckling of wide hyperelastic columns opens new opportunities for designing light-weight reusable energy-absorbing materials.

In this paper, we first develop a theory to precisely predict the quasi-static force–displacement response of a multi-layered column structure, unveiling the influence of the geometry of the columns and the number of layers on the energy-absorbing performance, and highlighting the high energy dissipation capacity of a multi-layered structure composed of wide columns exhibiting the snapping-back buckling. Next, we fabricate the multi-layered energy-absorbing architected materials by multi-material 3D printing and sacrificial molding. The wide columns are made of a silicone elastomer, a typical hyperelastic material that can undergo reversible large deformation in a rate-independent manner. We conduct static and drop tests to verify that the proposed architected materials are capable of absorbing impact energy while keeping the peak force below a safety threshold. Finally, we demonstrate that their mechanical responses can be widely tuned by the geometry and preloads.

2. Theory

The energy-absorbing of our proposed architected material is based on the snapping-back buckling of wide hyperelastic columns (Figure 1), which ensures that the proposed material is reusable and its energy-absorbing performance is rate-independent. When subjected to an axial displacement Δl or force F (Figure 1A), a column of an initial shear modulus μ , and a width-to-length ratio w/l , constrained by the clamped–

clamped boundary condition buckles at a critical loading condition. Using finite element (FE) analysis, we found that the buckling mode transitions from continuous, snapping-through to snapping-back as w/l increases (Figure 1B) (for details on the FE modeling, see Experimental Section; Figure S1, Supporting Information). For a column exhibiting the continuous buckling mode, both the force and displacement increase after the buckling point (the black curve in Figure 1B), so there is no hysteresis, and thus no energy dissipation, between the loading and unloading paths under both displacement-controlled and force-controlled loading. The columns exhibiting the snapping-through (the blue curve in Figure 1B) and snapping-back buckling modes (the red curve in Figure 1B) show a decreased and subsequently increased force after the buckling points, resulting in a hysteresis under force-controlled loading (shaded regions in Figure 1B). The enclosed area quantifies the normalized dissipated energy after a complete force-controlled loading and unloading cycle, which is also the maximum dissipated energy a column could achieve under displacement-controlled loading, $E_{\text{dis}}^{\text{max}}$, when an infinite number of such columns are connected in series.^[11,17,29,30,33] Clearly, $E_{\text{dis}}^{\text{max}}$ depends on the width-to-length ratio, and thereby buckling mode (Figure 1C). Although $E_{\text{dis}}^{\text{max}}$ changes non-monotonically as w/l increases, the snapping-back buckling mode ($0.24 < w/l < 0.36$) leads to a higher $E_{\text{dis}}^{\text{max}}$ than the snapping-through buckling mode ($0.10 < w/l < 0.24$). The decrease in $E_{\text{dis}}^{\text{max}}$ after $w/l = 0.32$ is due to the fact that the increase in the height of the hysteresis area becomes slower than the decrease in its width (Figure S2, Supporting Information).

We next establish a theory to quantitatively predict the dissipated energy E_{dis} of an architected material composed of n layers of axially-loaded columns exhibiting the snapping-through or snapping-back buckling mode, assuming that the structure can be simplified to n number of the same columns connected in series (Figure 2A). For such a column chain, the external force F equals the force F_i acting on each column, $F = F_i$, while the external displacement ΔL equals the sum of the displacement Δl_i of all the columns, $\Delta L = \sum_{i=1}^n \Delta l_i$. Each column can buckle independently, with the force (F_i)–displacement (Δl_i) relation predicted by FE analysis as shown in Figure 1B.

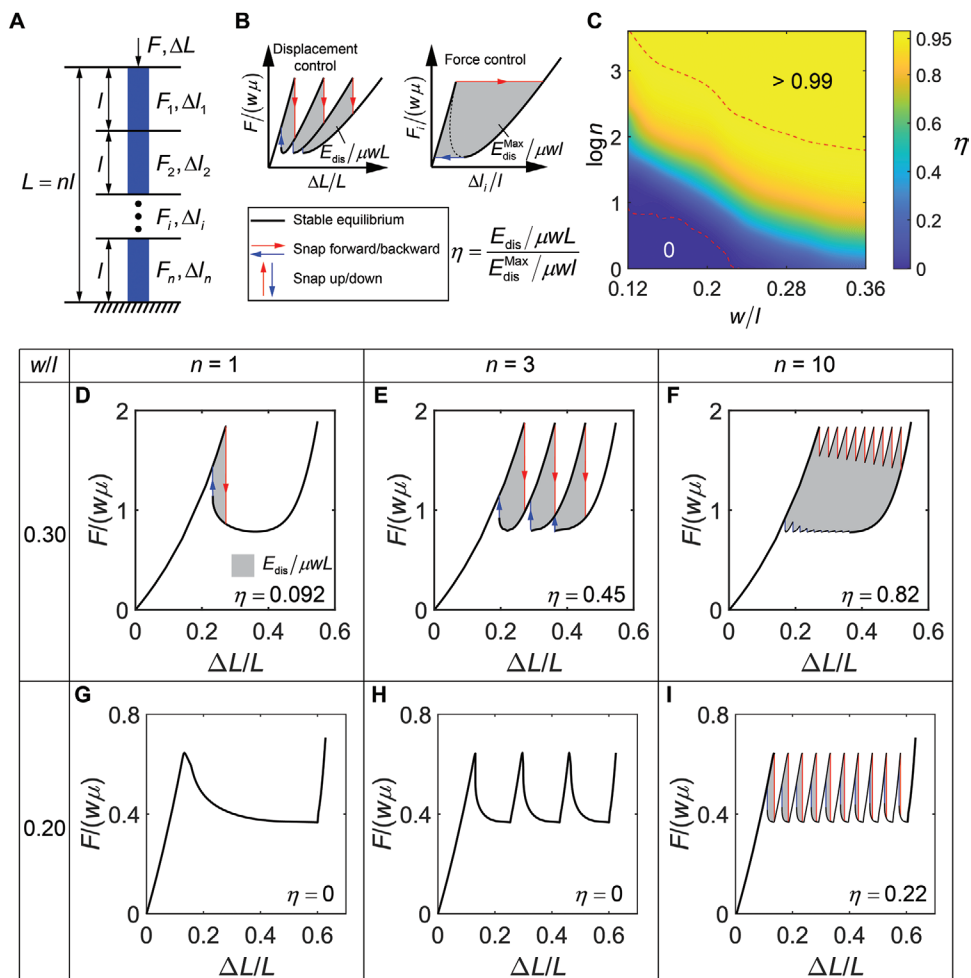


Figure 2. Energy dissipation of columns stacked in series. A) Schematic of n number of identical columns stacked in series. The whole structure is subjected to a compressive force F or a displacement ΔL . The force and displacement of each individual column are F_i and ΔL_i , respectively. B) Definition of the energy dissipation efficiency η , as the ratio of the normalized dissipated energy for a n -column chain system under displacement control, $E_{\text{dis}}/\mu w L$, to the maximum normalized energy that the same single column can dissipate, $E_{\text{dis}}^{\text{max}}/\mu w l$. C) The contour plot of η with respect to the number of columns n and the width-to-length ratio w/l of the columns. The two red dashed lines indicate the boundaries between the regions $\eta = 0$ and $0 < \eta \leq 0.99$, and between the regions $0 < \eta \leq 0.99$ and $\eta > 0.99$, respectively. D–I) The normalized force–displacement stable equilibrium paths (black), the snap-down (red), and snap-up (blue) paths under displacement control with the enclosed areas characterizing the dissipated energy (gray) for a n -column chain system containing columns with $w/l = 0.30$ (D–F) and 0.20 (G–I).

For a given force F , a column exhibiting snapping-through or snapping-back mode has at most three possible displacements ΔL_i . A column chain composed of n number of this identical column connected in series can thus have $C_{n+2}^2 = (n+1)(n+2)/2$ number of equilibrium F – ΔL branches (Text S1, Supporting Information).

Note that not every equilibrium branch is stable when the displacement ΔL is controlled externally. For a column chain composed of columns exhibiting the snapping-through buckling mode, its equilibrium branches are stable if either i) no column is in its negative-stiffness region (the negative slope part of its force–displacement curve), or ii) there is exactly one column in its negative-stiffness region while the overall force–displacement curve of the column chain has a negative slope.^[29,33] Otherwise, the equilibrium branches are unstable. For a column chain composed of columns exhibiting the snapping-back buckling mode, its stable equilibrium

branches can be determined by the following steps. Because a force–displacement curve featuring the snapping-back buckling is equivalent to the superposition of a monotonic force–displacement curve and a force–displacement curve featuring the snapping-through buckling (Figure S4, Supporting Information), we can view a column exhibiting the snapping-back buckling mode as a serial combination of a nonlinear elastic spring and a snapping-through element. We can then conceptually reorganize the column chain containing n snapping-back columns into n elastic springs and n snapping-through elements connected in series. We further replace the n elastic springs by a single spring with the equivalent force–displacement behavior. Therefore, the original column chain can be represented by a snapping-through element chain connected in series to a nonlinear elastic spring. Since the spring does not affect the stability, the stable equilibrium branches of this column chain can be identified using the same way as the

column chain composed of columns exhibiting the snapping-through buckling mode (Text S1, Supporting Information).

After the stable equilibrium branches are identified, the quasi-static loading and unloading F - ΔL relation under displacement control can be constructed. We plot the stable equilibrium F - ΔL paths of column chains composed of columns with $w/l = 0.30$ (Figure 2D–F) and 0.20 (Figure 2G–I), which exhibit the snapping-back and snapping-through buckling modes, respectively, and find that the paths are not always continuous. When the stable equilibrium paths are discontinuous (Figure 2D–F,I), that is, neighboring stable branches do not intersect, the column chain must snap rapidly down (red lines) or up (blue lines) to the neighboring stable equilibrium branch as one branch ends. The energy dissipated during a cycle of displacement-controlled loading is equal to the hysteresis area enclosed by the loading and unloading paths (grey areas), which is denoted by E_{dis} . If the stable equilibrium paths F - ΔL are continuous (Figure 2G,H), the force F varies smoothly along the paths as the column chain is loaded or unloaded under controlled ΔL , leading to zero energy dissipation.

To evaluate the performance of the energy dissipation for a column chain containing n number of columns under displacement-controlled loading, we define the energy dissipation efficiency η as the ratio of its normalized energy dissipation $E_{\text{dis}}/\mu wL$ (Figure 2B left) to the normalized maximum energy dissipation that one column in this column chain can achieve $E_{\text{dis}}^{\text{max}}/\mu wL$ (Figure 2B right) such that η ranges from 0 to 1. We plot the contour of η with respect to the number n and the width-to-length ratio w/l of the columns (Figure 2C). When w/l is low (corresponding to the snapping-through buckling mode), η equals zero before n reaches a threshold value (the lower red dashed line in Figure 2C), increases slowly with n beyond the threshold, and approaches 1 as n increases to a very large number (upper red dashed line in Figure 2C). To achieve a given η value, the number of layers n needed dramatically decreases with w/l . In particular, when w/l is high (corresponding to the snapping-back buckling mode), only less than 10 layers are needed to achieve η above 0.8, while tens of or even hundreds of layers are needed to reach the same η when w/l is low and in the snapping-through region. For example, η is nonzero when $n = 1$ (Figure 2D), equals 0.45 when $n = 3$ (Figure 2E), and reaches 0.82 when $n = 10$ (Figure 2F) for $w/l = 0.30$, whereas η remains zero when $n = 1$ (Figure 2G) and $n = 3$ (Figure 2H), and reaches merely 0.22 when $n = 10$ (Figure 2I) for $w/l = 0.20$. We further compare the energy dissipation of our material composed of wide columns to that of curved beams. We find that a wide column with $w/l = 0.30$ has maximum normalized dissipated energy $E_{\text{dis}}^{\text{max}}/\mu AL$ one order of magnitude higher than that of a curved beam with the optimal geometry^[17] (0.3015 for the wide beam shown in Figure S2A, Supporting Information, and 0.0266 for the curved beam shown in Figure S5A, B, Supporting Information). Moreover, the energy dissipation efficiency of a multi-layered structure composed of the wide columns is higher than that of the curved beam with the same number of layers (Figure S5C, Supporting Information). Therefore, compared to both the columns and the curved beams exhibiting a snapping-through buckling mode, those wide columns exhibiting the snapping-back buckling mode are better candidates for energy-absorbing elements, since not only a

single column has a higher maximum energy dissipation, but also less layers are needed to achieve the maximum energy dissipation.

3. Experiment

3.1. Fabrication and Characterization

We fabricated the multi-layered energy-absorbing architected materials composed of wide columns with required constraints to prevent shearing of the columns using multi-material 3D printing and sacrificial molding (Figure 3A). We 3D printed a mold, which consists of a stiff frame made of polylactic acid (PLA) and sacrificial parts made of polyvinyl alcohol by using a dual-extruder fused deposition modeling printer (Ultimaker S5). A pre-cured silicone elastomer was poured into the mold for curing, yielding elastomeric columns with an initial shear modulus $\mu = 16.46$ KPa (Experimental Section; Text S2, Supporting Information). To maintain the integrity of the material subjected to large compression, the columns are designed to be interconnected by wide flanges embedded into the frames (see the cross section view in Figure 3A). Subsequently, the mold was placed in water to dissolve the sacrificial parts. 3D printed hinges made of PLA were assembled to the structure to ensure that the columns exhibit the desired buckling mode when the material is loaded axially. Figure 3B shows a sample of an 8-layered architected material with 5×5 identical columns of a width-to-length ratio $w/l = 0.30$ in each layer. Each column has a width $w = 3$ mm, length $l = 10$ mm, and the out-of-plane thickness $b = 9$ mm. Upon a critical compression, the columns buckle and bend toward the width direction, exhibiting the snapping-back buckling modes (Figure 3C).

We conducted displacement-controlled loading and unloading tests (Experimental Section) for the sample shown in Figure 3B, and plotted the normalized loading and unloading force–displacement curves (Figure 3D). During loading, the layers buckle sequentially, which results in eight peaks in the loading path (the red curve in Figure 3D), each corresponding to the onset of buckling of one layer (Movie S1, Supporting Information). The force at each peak is the critical force for buckling of each layer F_{cr} . These peaks form a long and flat plateau of force, indicating large energy absorption at a near-constant load. Upon unloading, the layers recover sequentially, leading to eight peaks on the unloading path (the blue curve in Figure 3D, Movie S1, Supporting Information), prior to fully recovering its initial configuration. The area enclosed by the loading and unloading curves in Figure 3D is the normalized dissipated energy $E_{\text{dis}}/\mu AL$, with A the total area of all the columns $25wb$, while the area underneath the unloading curve is the normalized energy returned to the load head $E_{\text{ret}}/\mu AL$. We also found that the loading rates and the number of loading cycles have negligible effects on the energy dissipation due to the hyperelastic nature of the constitutive material (Figure S7, Supporting Information). Hence, the proposed architected material is reusable, rate-independent, and self-recoverable. The experimental result agrees well with the theoretical prediction on the number of force peaks and the width of the force plateau on both the loading and unloading curves, the

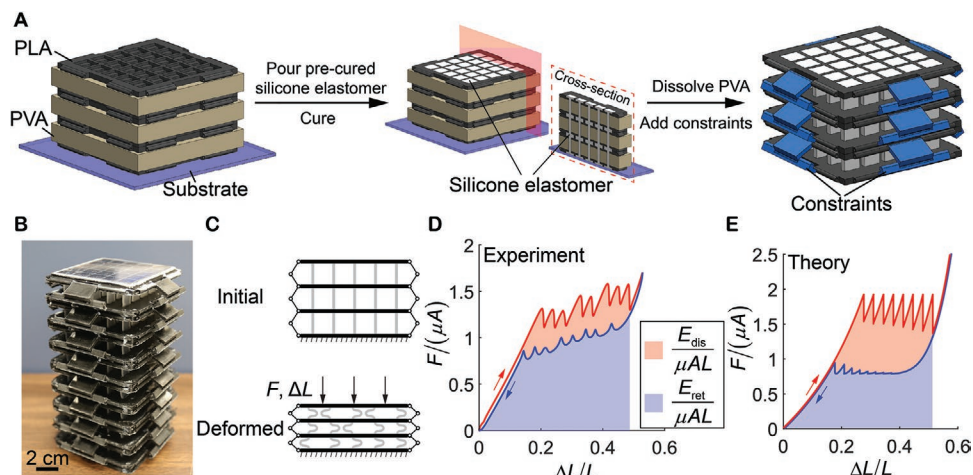


Figure 3. Fabrication process and mechanical responses of the proposed architected materials. A) Fabrication process of the proposed architected materials through multi-material 3D printing and sacrificial molding. B) A fabricated 8-layered architected material with 5×5 identical wide columns of a width-to-length ratio $w/l = 0.30$ in each layer. Each column has a width $w = 3$ mm, length $l = 10$ mm, and out-of-plane thickness $b = 9$ mm. C) Schematics of the initial and buckled states of the architected material when subjected to a compressive force F or a displacement ΔL . D, E) The displacement-controlled force–displacement response of the sample shown in (B) from the experiment (D) with the loading/unloading strain rate $\pm 0.2 \text{ min}^{-1}$ and the theory (E). The force is normalized by μA , with A the total area of all the columns $25wb$, while the displacement is normalized by L . The red curve denotes the loading path, whereas the blue curve denotes the unloading curve. The shaded area enclosed by the loading and unloading curves equals the normalized dissipated energy $E_{\text{dis}}/\mu AL$, while the shaded area underneath the unloading curve equals the normalized energy returned to the load head $E_{\text{ret}}/\mu AL$.

normalized plateau force on the unloading curve, and the returned energy (Figure 3E). However, the experimental result shows a lower F_{cr} for each layer, which is caused by unavoidable imperfections in the architected material. Besides, the bottom layers buckle at slightly lower F_{cr} than those of the top layers due to the preloads caused by gravity, leading to a slight increase in the force across the plateau as the displacement increases. The good agreement between the experiment (Figure 3D) and theory (Figure 3E) indicates that the behavior of the proposed material is highly predictable.

We further examined the performance of the proposed architected material during an impact by drop tests (Experimental Section). We simulate the situations where the protected object is placed at the top of the material whereas the impact occurs at its bottom. The peak force acting on the protected object is expected to be restrained below the safety threshold when certain level of impact energy is applied. We dropped an 8-layered sample containing columns of a width-to-length ratio $w/l = 0.30$, same as shown in Figure 3B, from different heights h , while measured the acceleration at its top surface using a piezoelectric accelerometer, and converted it to the force by multiplying the acceleration a by the mass of the top plate ($m = 0.156$ kg). To achieve a high input energy E_{inp} with a small height, we increased the total dropped weight by attaching some steel plates to the bottom of the sample (Figure S8, Supporting Information). As a result, we obtained E_{inp} up to 2.5 J within a height of 20 cm. We find that the peak force F_{peak} acting on the top plate remains almost a plateau in a broad range of E_{inp} , forming a force mitigation regime (Figure 4A). The force at this plateau matches the critical force measured in the static compression test, F_{cr} (ranging from 15.65 N at the first peak to 18.37 N at the eighth peak in Figure 3D), even though the strain rate in the drop test is 2×10^4 times higher than that in the static

test (Experimental Section). This remarkable agreement indicates that the proposed energy-absorbing mechanism is rate-independent. Besides, the force plateau occurs in the range of E_{inp} from 0.6 to 1.8 J, which is on the same order of magnitude as the absorbed energy underneath the plateau of the force–displacement loading path in the static test (0.45 J, Figure 3D). The level of the force plateau and the corresponding range of E_{inp} can be scaled up by increasing the modulus of the elastomer and the number of columns in each layer. Figure 4B shows the acceleration–time relation when an impact energy of $E_{\text{inp}} = 1.8$ J (upper limit of the mitigation regime) is applied. During the impact, the columns buckle sequentially from the bottom layer to the top layer (Figure 4C1–C3; Movie S2, Supporting Information), limiting the impact force acting on the top layer to the critical force for column buckling. The drop tests confirm that the proposed architected materials are capable of restraining the impact force from exceeding the safety threshold for a wide scope of input energy at high strain rates by harnessing the snapping-back buckling.

3.2. Programmable Behavior of the Architected Material

The performance of the proposed architected material can be programmed by the width-to-length ratio w/l of the columns. According to Figure 2C, the materials with low w/l show no energy dissipation if the number of layers n is not large enough. We built an 8-layered architected material with 5×5 identical columns of $w/l = 0.14$ in each layer (Experimental Section). This material is expected to have zero energy dissipation based on our theory (Figure 5B). We conducted a displacement-controlled loading and unloading test for this sample (Experimental Section), and found that the loading and unloading

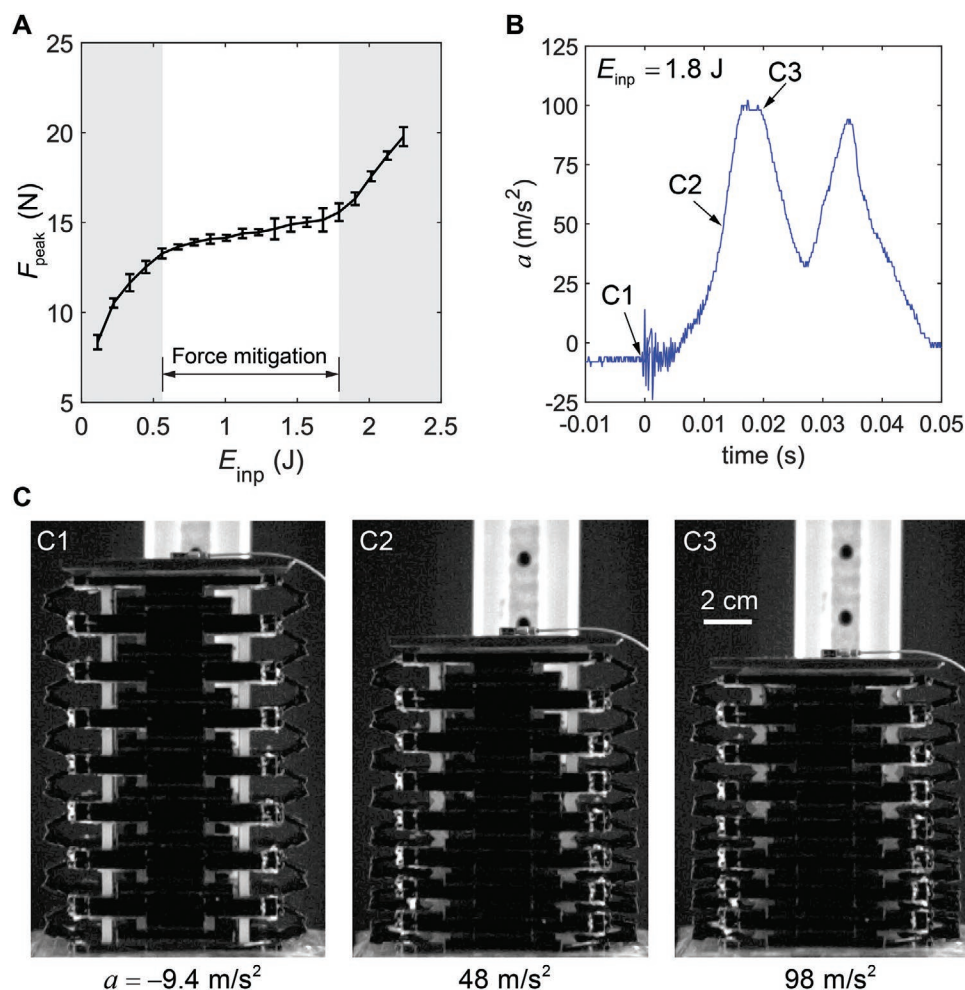


Figure 4. Drop tests for the proposed architected material. A) The peak reaction force F_{peak} on the top surface as a function of the input energy E_{inp} from the bottom. The error bars indicate the standard deviations of five tests for a given E_{inp} . The force remains nearly constant in a wide range of E_{inp} in the force mitigation regime. B) Acceleration–time relation during the impact when $E_{inp} = 1.8$ J. C) Snapshots of the sample corresponding to the three time points in (B). C1) The moment when the impact occurs. C2) The lower layers have buckled whereas the upper layers remain unbuckled. C3) The deformation at the peak acceleration, where all layers have buckled. The measured accelerations at the top surface are labeled at the bottom of all the snapshots. The negative sign indicates that the direction of the acceleration is vertically downward.

curves are very close, resulting in very small energy dissipation $E_{dis}/\mu AL = 0.0087$ (Figure 5A; Movie S3, Supporting Information). This energy dissipation is negligible compared to the energy dissipated in the 8-layered architected material with columns of $w/l = 0.30$ (Figure S9, Supporting Information). The small energy dissipation observed is potentially caused by the adhesion in the self-contact region as the columns are fully folded.^[31]

Besides, the critical force for buckling of each layer and the ratio of dissipated energy to returned energy can be tuned by preloads. We hung some weight balances to the sample shown in Figure 3B as a preload (Figure S10, Supporting Information). As the preload increases, both the critical force and the returned energy are reduced, but the dissipated energy is maintained (Figure 5C,D; Movies S4, Supporting Information). Hence, the ratio of the dissipated energy to the returned energy is increased. Remarkably, when the preload is large enough such that the unloading path is shifted below the zero force, this material can be transformed from monostable to bistable. As

shown by our experiment and theory (Figure 5E,F), instead of recovering to its original configuration, this material retains its deformed but stable configuration after unloading (Movie S5, Supporting Information), resulting in part of input energy trapped in the material.

4. Conclusion

In summary, we combine FE simulations, theoretical analysis, and experiments to develop a reusable energy-absorbing architected material harnessing the snapping-back buckling of wide hyperelastic columns. The quasi-static cyclic loading tests confirm that the proposed material is capable of dissipating energy while keeping the force nearly constant with a long working distance in a reusable, self-recoverable, and highly predictable manner, while the drop tests at high strain rates show the feature of rate-independency and the capability of force attenuation in a broad range of input

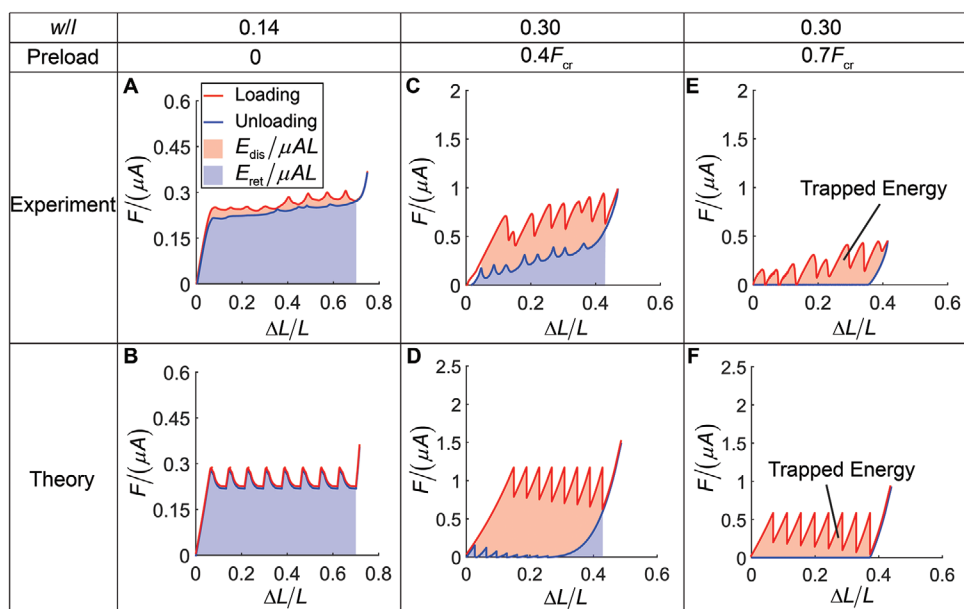


Figure 5. Influence of the width-to-length ratio w/l and the preloads on the performance of the proposed architected material. A,B) The displacement-controlled force–displacement response of an 8-layered architected material with columns of $w/l = 0.14$ from the experiment (A) and the theory (B). Each column has a width $w = 1.4$ mm, length $l = 10$ mm, and out-of-plane thickness $b = 9$ mm. C–F) The displacement-controlled force–displacement response of the sample shown in Figure 2B with a preload $0.4F_{cr}$ (C,D) and preload $0.7F_{cr}$ (E,F), with F_{cr} corresponding to the first peak force on the force–displacement loading curve when no preload is applied. The results from the experiments (A,C,E) and theory (B,D,F) agree well with each other.

energy. Moreover, we have demonstrated that the mechanical responses of the proposed energy-absorbing material can be widely tuned by the geometry and preloads. Compared to a multi-layered material harnessing the snapping-through buckling, ours harnessing the snapping-back buckling has higher maximum dissipation energy, and requires much less layers to achieve the maximum dissipation energy, which can dramatically reduce the volume and mass of the material for the same energy-absorbing performance. Due to the high local strain during the snapping-back buckling, our design of wide columns is limited to hyperelastic elastomers. Our findings broaden the design strategies for reusable energy-absorbing materials in applications including crashworthiness improvement of vehicles and aircrafts, protective packaging in goods transportation, and personal safety devices in sports.

5. Experimental Section

Finite Element Modeling: The commercial software Abaqus/Standard was used for static finite element simulations. The static Riks method was implemented to capture the unstable equilibrium force–displacement responses. Columns were modeled as an incompressible neo-Hookean material in plane strain conditions with hybrid quadratic rectangular elements (Abaqus type CPE8H). Defects with very small sizes were introduced to trigger buckling and creasing instabilities (Figure S1, Supporting Information). The size of the imperfection for buckling was $\Delta d/w = 0.001$, and the size of the imperfection for creasing was $r/w = 0.002$. A mesh refinement study was performed to ensure the mesh size was at least one order of magnitude smaller than the dimension of the finest part of the samples. As a result, approximately from 6×10^4 to 4×10^5 quadrilateral elements were involved in each finite element model, depending on the width-to-length ratio of columns.

Fabrication: The samples were fabricated by molding silicone elastomers into the 3D printed molds. Ecoflex 00-30 was used for the samples containing columns with a width-to-length ratio $w/l = 0.30$, SORTA-Clear 40, which has a modulus over 10 times higher than the Ecoflex 00-30, was used for the samples containing columns with $w/l = 0.14$. As a result, these samples with two different w/l had similar critical forces for column buckling. The characterization of the moduli of the two silicone elastomers is shown in Text S2, Supporting Information.

Static Tests: A uniaxial testing machine (Instron 5966) with a 500 N load cell was used to measure the displacement-controlled force–displacement relations of the proposed architected materials. The experimental results shown in Figures 3,5 were obtained at a strain rate of $\pm 0.2 \text{ min}^{-1}$ (16 mm min^{-1}). During the tests, the deformation of the samples was recorded by a Canon EOS 6D digital SLR camera. To investigate the effect of the number of loading cycles on the mechanical behavior of the samples, 50 loading and unloading compressive tests at a strain rate $\pm 0.2 \text{ min}^{-1}$ were conducted for the samples shown in Figure 3B. To explore whether the behavior was rate-dependent, the tests at strain rates ranging from ± 0.05 to $\pm 1 \text{ min}^{-1}$ were conducted.

Drop Tests: To explore the energy-absorbing performance of the proposed architected material, the sample was dropped from different heights to create impacts at its bottom, while measured the impact force at its top. The setup of the drop tests is shown in Figure S8, Supporting Information. The sample together with some steel plates attached to its bottom was dropped from different heights h ranging from 1 to 20 cm. The total weight dropped was 1.142 kg. A slider on a rail was used to guide the fall of the sample. A piezoelectric accelerometer (PCB Piezotronics, Inc., model number: 352C23) was attached onto the top plate on the sample to record its acceleration. The impact force can be calculated by multiplying the acceleration by the mass of the top plate ($m = 0.156 \text{ kg}$). The drop test was recorded using a Phantom V7.2 high speed camera at 6600 frames per second. The Movie S2, Supporting Information shows the deformation process of the sample during the impact. This movie is played at 100 frame per second, which is 66 times slower than the actual time scale. From this movie, it can be seen the strain rate is roughly 4000 min^{-1} , which is 20 000 times higher than the strain rate in the static tests.

Supporting Information

Supporting Information is available from the Wiley Online Library or from the author.

Acknowledgements

This work was supported by the startup fund from Henry Samueli School of Engineering and Applied Science at University of California, Los Angeles (UCLA) and Hellman fellowship. This work used computational and storage services associated with the Hoffman2 Shared Cluster provided by Institute for Digital Research and Education's Research Technology Group at UCLA. The authors thank Dr. Chang-Jin Kim at UCLA for providing the high-speed camera. The authors also thank Dr. Vijay Gupta at UCLA for providing the amplifier and the oscilloscope.

Conflict of Interest

The authors declare no conflict of interest.

Author Contributions

Y.C. and L.J. designed the study. Y.C. carried out the simulations and experiments. Y.C. and L.J. analyzed the data and wrote the manuscript.

Data Availability Statement

The data that support the findings of this study are available from the corresponding author upon reasonable request.

Keywords

architected material, energy dissipation, energy-absorbing material, rate-independent, reusable, self-recoverable, snapping-back buckling

Received: March 3, 2021

Revised: April 17, 2021

Published online:

-
- [1] L. J. Gibson, M. F. Ashby, *Cellular Solids: Structure and Properties*, Cambridge University Press, Cambridge **1999**.
 [2] L. Salari-Sharif, T. A. Schaedler, L. Valdevit, *J. Mater. Res.* **2014**, *29*, 1755.
 [3] G. Lu, T. X. Yu, *Energy Absorption of Structures and Materials*, Woodhead Publishing, Cambridge **2003**.

- [4] M. C. Constantinou, M. Symans, *Experimental and Analytical Investigation of Seismic Response of Structures with Supplemental Fluid Viscous Dampers*, National Center For Earthquake Engineering Research, Buffalo, NY **1992**.
 [5] L. Wang, J. Lau, E. L. Thomas, M. C. Boyce, *Adv. Mater.* **2011**, *23*, 1524.
 [6] P. Zhang, M. A. Heyne, A. C. To, *J. Mech. Phys. Solids* **2015**, *83*, 285.
 [7] R. Wang, J. Shang, X. Li, Z. Luo, W. Wu, *Sci. Rep.* **2018**, *8*, 9604.
 [8] J. M. Bajkowski, B. Dyniewicz, C. I. Bajer, *Mech. Syst. Signal Process.* **2016**, *70*, 387.
 [9] K. Fu, Z. Zhao, L. Jin, *Adv. Funct. Mater.* **2019**, *29*, 1901258.
 [10] Y. Wang, B. Ramirez, K. Carpenter, C. Naify, D. C. Hofmann, C. Daraio, *Extreme Mech. Lett.* **2019**, *33*, 100557.
 [11] D. Restrepo, N. D. Mankame, P. D. Zavattieri, *Extreme Mech. Lett.* **2015**, *4*, 52.
 [12] S. Shan, S. H. Kang, J. R. Raney, P. Wang, L. Fang, F. Candido, J. A. Lewis, K. Bertoldi, *Adv. Mater.* **2015**, *27*, 4296.
 [13] D. M. Correa, T. Klatt, S. Cortes, M. Haberman, D. Kovar, C. Seepersad, *Rapid Prototyp. J.* **2015**, *21*, 193.
 [14] A. Rafsanjani, A. Akbarzadeh, D. Pasini, *Adv. Mater.* **2015**, *27*, 5931.
 [15] B. Haghpanah, L. Salari-Sharif, P. Pourrajab, J. Hopkins, L. Valdevit, *Adv. Mater.* **2016**, *28*, 7915.
 [16] A. Rafsanjani, D. Pasini, *Extreme Mech. Lett.* **2016**, *9*, 291.
 [17] T. Frenzel, C. Findeisen, M. Kadic, P. Gumbsch, M. Wegener, *Adv. Mater.* **2016**, *28*, 5865.
 [18] N. Kidambi, R. L. Harne, K. W. Wang, *Smart Mater Struct.* **2017**, *26*, 085011.
 [19] C. S. Ha, R. S. Lakes, M. E. Plesha, *Mater. Des.* **2018**, *141*, 426.
 [20] H. Yang, L. Ma, *Mater. Des.* **2018**, *152*, 181.
 [21] F. Pan, Y. Li, Z. Li, J. Yang, B. Liu, Y. Chen, *Adv. Mater.* **2019**, *31*, 1900548.
 [22] C. Morris, L. Bekker, C. Spadaccini, M. Haberman, C. Seepersad, *Adv. Eng. Mater.* **2019**, *21*, 1900163.
 [23] H. Yang, L. Ma, *J. Mater. Sci.* **2019**, *54*, 3509.
 [24] Y. Zhang, D. Restrepo, M. Velay-Lizancos, N. D. Mankame, P. D. Zavattieri, *Sci. Rep.* **2019**, *9*, 12581.
 [25] Y. Zhang, Q. Wang, M. Tichem, F. van Keulen, *Extreme Mech. Lett.* **2020**, *34*, 100593.
 [26] E. G. Karpov, D. Ozevin, M. Mahamid, L. A. Danso, *Int. J. Solids Struct.* **2020**, *199*, 158.
 [27] Z. Vangelatos, A. Micheletti, C. P. Grigoropoulos, F. Fraternali, *Nanomaterials* **2020**, *10*, 652.
 [28] S. Sun, N. An, G. Wang, M. Li, J. Zhou, *Appl. Phys. Lett.* **2019**, *115*, 091901.
 [29] G. Puglisi, L. Truskinovsky, *J. Mech. Phys. Solids* **2000**, *48*, 1.
 [30] B. Haghpanah, A. Shirazi, L. Salari-Sharif, A. G. Izard, L. Valdevit, *Extreme Mech. Lett.* **2017**, *17*, 56.
 [31] Y. Chen, L. Jin, *Extreme Mech. Lett.* **2020**, *34*, 100600.
 [32] Y. Chen, L. Jin, *Int. J. Non-Linear Mech.* **2020**, *125*, 103532.
 [33] I. Benichou, S. Givli, *J. Mech. Phys. Solids* **2013**, *61*, 94.